

Cite this: *Chem. Sci.*, 2025, 16, 22348

All publication charges for this article have been paid for by the Royal Society of Chemistry

# Fluorine-mediated single-step ethylene purification in face-transitive metal–organic frameworks from binary to ternary gas mixtures

Wei-Hong Zhang, Ya-Nan Ma, Guo-Tong Du, Ping Wang and Dong-Xu Xue \*

Ethylene is a pivotal feedstock for the chemical industry. Obtaining polymer-grade ethylene in a single step from either binary ethane/ethylene or ternary acetylene/ethane/ethylene mixtures *via* porous adsorbents is highly energy-efficient yet remains a formidable challenge. Face-transitive topologies, a particular class of nets in reticular chemistry, possess only one window type and thus hold exceptional promise for discriminating between closely related C<sub>2</sub> hydrocarbons. Guided by the *nia-d* topology, we synthesized two isorecticular, trinuclear-manganese-cluster-based, ternary metal–organic frameworks (MOFs), namely *nia-d*-TZB and *nia-d*-FTZB, under solvothermal conditions using MnCl<sub>2</sub>, the tritopic linker 2,4,6-tri(4-pyridyl)-1,3,5-triazine (TPT), and the heterofunctional linear linkers 4-(1*H*-tetrazol-5-yl)benzoic acid (H<sub>2</sub>TZB) or 2-fluoro-4-(1*H*-tetrazol-5-yl)benzoic acid (H<sub>2</sub>FTZB). Although the resultant trigonal-bipyramidal cages remain dimensionally invariant, the introduction of fluorine in the latter linker subtly reduces the size of the antiprismatic cages and the sole triangular window in *nia-d*-FTZB. Single-component adsorption isotherms reveal that *nia-d*-TZB preferentially adsorbs ethane, whereas *nia-d*-FTZB preferentially adsorbs both acetylene and ethane. Consequently, *nia-d*-TZB enables one-step purification of ethylene from an ethane/ethylene mixture, while *nia-d*-FTZB achieves simultaneous removal of acetylene and ethane from an acetylene/ethane/ethylene ternary stream, again delivering polymer-grade ethylene in a single pass. These findings are corroborated by ideal adsorbed solution theory (IAST), breakthrough experiments with both binary and ternary gas mixtures, and detailed theoretical simulations. This study furnishes compelling evidence for the rational design of face-transitive MOFs to tackle complex gas-separation tasks.

Received 4th September 2025  
Accepted 6th October 2025

DOI: 10.1039/d5sc06836c

rsc.li/chemical-science

## Introduction

Ethylene (C<sub>2</sub>H<sub>4</sub>), a cornerstone of the modern petrochemical industry with an annual global production exceeding 200 million tons, serves as the primary feedstock for polyethylene and other commodity chemicals. Currently, industrial C<sub>2</sub>H<sub>4</sub> production relies on the processes such as naphtha steam cracking and ethane dehydrogenation, which inevitably generate by-products like acetylene (C<sub>2</sub>H<sub>2</sub>) and ethane (C<sub>2</sub>H<sub>6</sub>). Achieving polymer-grade ethylene (purity > 99.9%) demands complete removal of these impurities. Conventional purification employs a multi-step approach: selective hydrogenation of C<sub>2</sub>H<sub>2</sub> using noble-metal catalysts (*e.g.*, Pd) followed by cryogenic distillation to separate C<sub>2</sub>H<sub>4</sub>/C<sub>2</sub>H<sub>6</sub>.<sup>1–4</sup> However, this process suffers from excessive energy consumption (distillation operates at high pressure and subzero temperatures) and environmental burdens. The challenge is further exacerbated by the

overlapping boiling points (184.6 K, 188.4 K, and 169.4 K for C<sub>2</sub>H<sub>6</sub>, C<sub>2</sub>H<sub>2</sub>, and C<sub>2</sub>H<sub>4</sub>, respectively), rendering traditional separation methods inefficient. Adsorptive separation employing porous materials offers a highly promising, energy-efficient alternative to conventional methods.<sup>5</sup>

Metal–organic frameworks (MOFs), as a class of emerging crystalline porous materials, have attracted intensive attention from the scientific community to industry over the past two decades.<sup>6–10</sup> These materials combine facile synthesis, well-defined structures, tunable functionalities, and rich chemical diversity, endowing them with broad potential across gas storage,<sup>11–18</sup> separation,<sup>19–24</sup> catalysis,<sup>25–29</sup> sensing,<sup>30–36</sup> pharmaceutical delivery<sup>37,38</sup> and so on. In particular, MOFs have achieved notable progress in ethylene purification. Current reports on ethylene purification primarily address binary gas separations, namely ethylene/acetylene and ethylene/ethane mixtures, as well as ternary gas separations, *i.e.*, ethylene/acetylene/ethane mixtures.<sup>39–44</sup> In binary ethylene/ethane separations, ethane-selective adsorbents have garnered considerable interest in recent years because they enable direct, single-step ethylene purification with reduced energy expenditure by avoiding secondary desorption steps.<sup>45,46</sup> Given that the kinetic

Shaanxi Provincial Key Laboratory of New Concept Sensors and Molecular Materials, Key Laboratory of Applied Surface and Colloid Chemistry of Ministry of Education, School of Chemistry & Chemical Engineering, Shaanxi Normal University, Xi'an 710119, China. E-mail: xuedx@snnu.edu.cn



diameters, the quadrupole moment and polarizability of ethylene (C<sub>2</sub>H<sub>4</sub>: 4.16 Å, approximately  $1.5 \times 10^{-26}$  esu cm<sup>2</sup> and  $42.5 \times 10^{-25}$  cm<sup>3</sup>, respectively) lie between those of acetylene (C<sub>2</sub>H<sub>2</sub>: 3.33 Å,  $7.2 \times 10^{-26}$  esu cm<sup>2</sup> and  $39.3 \times 10^{-25}$  cm<sup>3</sup>, respectively) and ethane (C<sub>2</sub>H<sub>6</sub>: 4.44 Å,  $0.65 \times 10^{-26}$  esu cm<sup>2</sup> and  $44.7 \times 10^{-25}$  cm<sup>3</sup>, respectively), achieving simultaneous removal of acetylene and ethane from a C<sub>2</sub> mixture to yield one-step ethylene purification from the three-component ethylene/acetylene/ethane feed remains exceptionally challenging.<sup>47</sup> In recent years, numerous MOF materials have been reported that enable one-step purification of ethylene from both two-component<sup>48–56</sup> and three-component C<sub>2</sub> mixtures.<sup>57–64</sup> Nevertheless, the design and synthesis of new MOFs that combine high selectivity with large uptake remains highly anticipated within the community.

Topology-guided reticular chemistry plays a crucial role in the design and synthesis of MOFs.<sup>65–68</sup> In particular, MOF networks with a single window are referred to as face-transitive.<sup>69</sup> The window serves as the sole gateway for gas molecules to enter and exit the internal cavities. Consequently, structures featuring only a single window are more readily tunable during bottom-up assembly. As a result, the regulated synthesis of face-transitive MOFs has emerged as an effective strategy to address efficient gas separations. Among them, **nia-d**, also known as **pacs**, is a (3,9)-c topology with a transitivity of 2212.<sup>70</sup> This notation indicates that the network contains two kinds of vertices, two kinds of edges, one kind of face (window), and two kinds of tiles (cavities), thereby constituting a face-transitive network. In recent years, **nia-d/pacs**-type network has attracted considerable attention from numerous research groups for its potential in guiding high-performance gas separation MOFs.<sup>71–77</sup>

Building on the above findings and the isorecticular chemistry strategy, we report the synthesis of two **nia-d**-type trinuclear manganese-based MOFs using the same metal source and a tridentate triazine ligand, as well as a hetero-functional linear linker bearing carboxylic acid and tetrazole motifs. One linker is fluorine-free, while the side arm of the carboxylate in the other linker is fluorinated. Notably, these two materials exhibit distinct adsorption behaviours toward C<sub>2</sub> hydrocarbons, leading to different separation performances. The synthesis and structure, as well as the adsorption and separation properties, breakthrough measurements with mixed C<sub>2</sub> feeds, and mechanistic interpretations, are described in detail below.

## Results and discussion

### Synthesis and structure

Indeed, solvothermal reactions at 135 °C in DMF solvent combining MnCl<sub>2</sub> with 2,4,6-tri(4-pyridyl)-1,3,5-triazine (TPT) and either 4-(1*H*-tetrazol-5-yl)benzoic acid (H<sub>2</sub>TZB) or 2-fluoro-4-(1*H*-tetrazol-5-yl)benzoic acid (H<sub>2</sub>FTZB) with trifluoroacetic acid as additive yielded yellow hexagonal-prismatic single crystals. Single-crystal X-ray diffraction (SCXRD), together with dye exchange experiments and X-ray photoelectron spectroscopy (XPS) (Fig. S3–S6), established the molecular formulae as [Mn<sup>II</sup>Mn<sup>III</sup>(μ<sub>3</sub>-O)(TZB)<sub>3</sub>TPT]·x(solvent) for **nia-d**-TZB and

[Mn<sup>II</sup>Mn<sup>III</sup>(μ<sub>3</sub>-O)(FTZB)<sub>3</sub>TPT]·x(solvent) for **nia-d**-FTZB. SCXRD reveals that **nia-d**-TZB and **nia-d**-FTZB are isorecticular (Tables S4 and S5), both crystallizing in the hexagonal space group *P6<sub>3</sub>/mmc*. In both structures, linear linkers yield the well-known 6-c **acs** network. The hexagonal channels are then sequentially occupied by triangular TPT linkers that cap the exposed [Mn<sub>3</sub>(μ<sub>3</sub>-O)] clusters, leading to the intended (3,9)-c **nia-d** topological 3-periodic framework.

Two distinct cage motifs are present in both compounds, *i.e.*, a triangular bipyramidal cage (cage-I) and an anti-prismatic cage (cage-II). The dimensions of cage-I are  $9.96 \times 16.15$  Å<sup>2</sup> in both structures. The presence of fluorine in the linear linker slightly perturbs cage-II, changing its dimensions from  $13.17 \times 6.30$  Å<sup>2</sup> in **nia-d**-TZB to  $12.62 \times 6.23$  Å<sup>2</sup> in **nia-d**-FTZB (Fig. 1). At the same time, the triangular windows, defined by portions of the TPT linker and two linear linkers, serve as the sole entrances/exits for the framework. The aperture size modestly decreases from 5.16 Å in **nia-d**-TZB to 5.0 Å in **nia-d**-FTZB (Fig. S2). Nevertheless, these window dimensions remain sufficient to permit the passage of C<sub>2</sub> gas molecules.

### Porosity, adsorption and separation

The solvent-accessible pore volumes for **nia-d**-TZB and **nia-d**-FTZB are 57.9% and 54.2%, respectively. The excellent agreement between bulk powder X-ray diffraction (PXRD) patterns and single-crystal simulations confirms the phase purity of the synthesized materials (Fig. S12 and S13). To assess porosity, the two samples were subjected to three days of consecutive exchanges with acetonitrile or acetone, followed by evacuation at 120 °C under vacuum prior to adsorption measurements. Nitrogen sorption isotherms measured at 77 K display Type-I behaviour for both samples, consistent with their microporous character. At 1 bar, **nia-d**-TZB ( $546 \text{ cm}^3 \text{ g}^{-1}$ ) exhibits a higher nitrogen uptake than **nia-d**-FTZB ( $503 \text{ cm}^3 \text{ g}^{-1}$ ) (Fig. 2 and S7). Correspondingly, the BET surface areas and pore volumes are  $2029 \text{ m}^2 \text{ g}^{-1}$  and  $0.85 \text{ cm}^3 \text{ g}^{-1}$ , respectively, for **nia-d**-TZB, and  $1987 \text{ m}^2 \text{ g}^{-1}$  and  $0.78 \text{ cm}^3 \text{ g}^{-1}$ , respectively, for **nia-d**-FTZB, which are consistent with their respective theoretical pore volumes of  $0.85 \text{ cm}^3 \text{ g}^{-1}$  and  $0.77 \text{ cm}^3 \text{ g}^{-1}$ , thereby confirming that the materials were fully activated. The pore size distributions are centered at 11.5 Å and 11.0 Å, respectively (Fig. S8). These results are in good agreement with the pore architectures inferred from the single-crystal structures, indicating that both materials were successfully activated and preserved their structural integrity.

To probe the C<sub>2</sub> gas adsorption behaviour, we collected a series of static sorption isotherms for **nia-d**-TZB and **nia-d**-FTZB. As shown in Fig. 3a, both materials exhibit higher uptake for ethane and acetylene than for ethylene. Specifically, at 298 K and 1 bar, the uptakes are  $143.72 \text{ cm}^3 \text{ g}^{-1}$  for C<sub>2</sub>H<sub>6</sub>,  $124.46 \text{ cm}^3 \text{ g}^{-1}$  for C<sub>2</sub>H<sub>2</sub>, and  $107.42 \text{ cm}^3 \text{ g}^{-1}$  for C<sub>2</sub>H<sub>4</sub> in **nia-d**-TZB. These uptakes are consistent with the zero-coverage isosteric heats of adsorption (*Q*<sub>st</sub>), *i.e.*, 29.85 kJ mol<sup>-1</sup> (C<sub>2</sub>H<sub>6</sub>), 27.88 kJ mol<sup>-1</sup> (C<sub>2</sub>H<sub>2</sub>), and 26.19 kJ mol<sup>-1</sup> (C<sub>2</sub>H<sub>4</sub>) (Fig. 3c and S16). Notably, the ethane uptake for **nia-d**-TZB reaches  $6.42 \text{ mmol g}^{-1}$ , a value higher than those of many benchmark ethane-selective



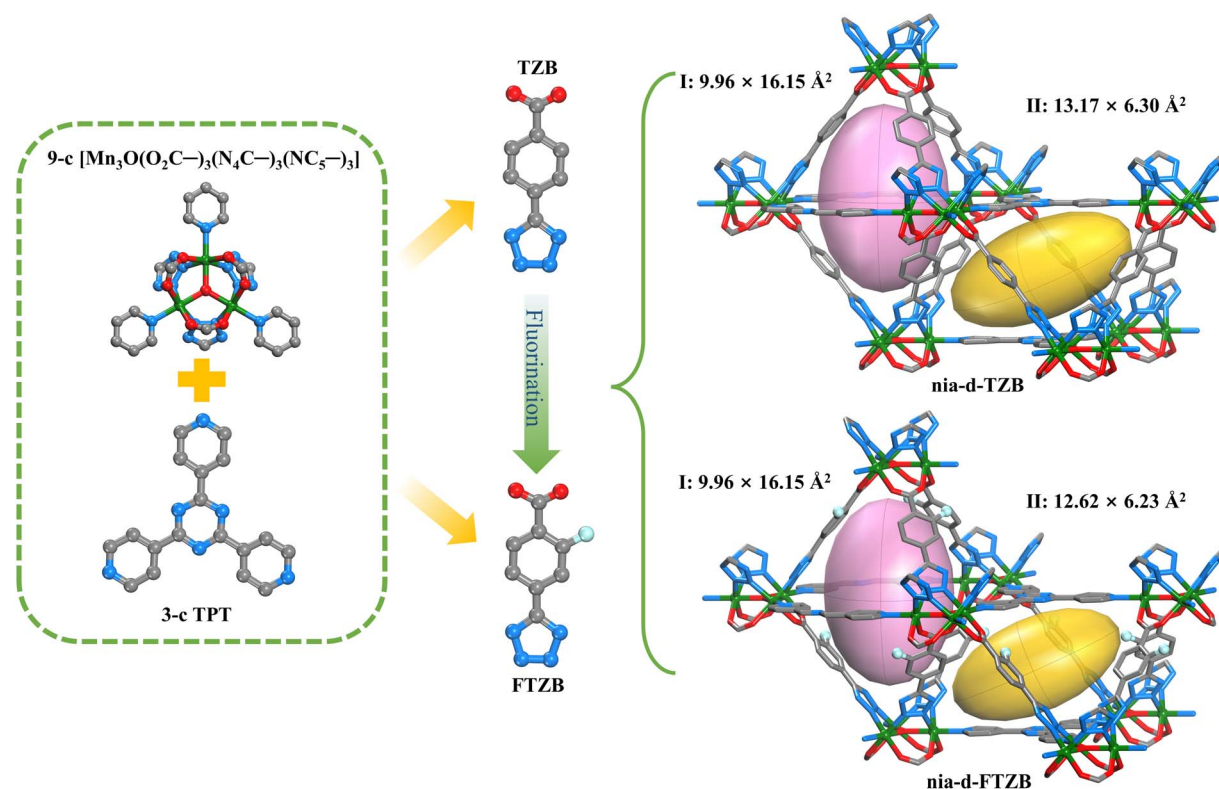


Fig. 1 Schematic representation of the two MOFs constructed from a trinuclear manganese cluster and respective mixed linkers associated with corresponding cage sizes. C: gray, Mn: green, O: red, N: sky blue, and F: light blue. Hydrogen atoms are omitted for clarity.

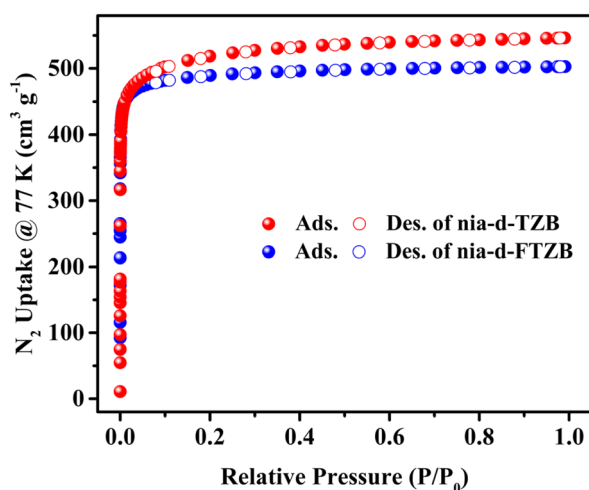


Fig. 2 The N<sub>2</sub> sorption isotherms at 77 K for nia-d-TZB and nia-d-FTZB.

adsorbents, such as PCN-250 (5.21 mmol g<sup>-1</sup>),<sup>78</sup> Ni-MOF-2 (5.94 mmol g<sup>-1</sup>),<sup>55</sup> MOF-303 (5.01 mmol g<sup>-1</sup>),<sup>79</sup> and UiO-67-(NH<sub>2</sub>)<sub>2</sub> (5.32 mmol g<sup>-1</sup>).<sup>80</sup> The C<sub>2</sub>H<sub>6</sub>/C<sub>2</sub>H<sub>4</sub> and C<sub>2</sub>H<sub>2</sub>/C<sub>2</sub>H<sub>4</sub> uptake ratios are 1.34 and 1.16, respectively. It is noteworthy that the adsorption isotherms for C<sub>2</sub>H<sub>2</sub> and C<sub>2</sub>H<sub>4</sub> are very close at low pressure, and the C<sub>2</sub>H<sub>2</sub>/C<sub>2</sub>H<sub>4</sub> uptake ratio is relatively low. Collectively, **nia-d-TZB** demonstrates a pronounced ethane-

selective adsorption behaviour toward C<sub>2</sub> gas mixtures, which is advantageous for the removal of ethane from binary C<sub>2</sub>H<sub>6</sub>/C<sub>2</sub>H<sub>4</sub> feeds and enables one-step purification of ethylene.

As for **nia-d-FTZB**, the introduction of fluorine markedly alters its adsorption profile, yielding the highest uptake for acetylene among the C<sub>2</sub> molecules studied. Specifically, at 298 K and 1 bar, the uptakes are 162.98 cm<sup>3</sup> g<sup>-1</sup> for C<sub>2</sub>H<sub>2</sub>, 140.94 cm<sup>3</sup> g<sup>-1</sup> for C<sub>2</sub>H<sub>6</sub>, and 125.69 cm<sup>3</sup> g<sup>-1</sup> for C<sub>2</sub>H<sub>4</sub> (Fig. 3b). The corresponding zero-coverage Q<sub>st</sub> is 29.98 kJ mol<sup>-1</sup> (C<sub>2</sub>H<sub>2</sub>), 29.53 kJ mol<sup>-1</sup> (C<sub>2</sub>H<sub>6</sub>), and 27.95 kJ mol<sup>-1</sup> (C<sub>2</sub>H<sub>4</sub>) (Fig. 3c and S17). The ethane uptake remains notably high, and although the ethylene uptake also increases, the C<sub>2</sub>H<sub>2</sub> isotherm lies above the C<sub>2</sub>H<sub>4</sub> isotherm within 0–1.0 bar. The C<sub>2</sub>H<sub>2</sub>/C<sub>2</sub>H<sub>4</sub> uptake ratio increases to 1.30. These data indicate that **nia-d-FTZB** exhibits concurrent selective adsorption of both acetylene and ethane, suggesting its potential for simultaneous removal of C<sub>2</sub>H<sub>2</sub> and C<sub>2</sub>H<sub>6</sub> from ternary C<sub>2</sub> feeds and enabling one-step purification of ethylene.

To assess the gas separation performance of **nia-d-TZB** and **nia-d-FTZB**, we calculated the selectivities for binary mixtures of C<sub>2</sub>H<sub>2</sub>/C<sub>2</sub>H<sub>4</sub> and C<sub>2</sub>H<sub>6</sub>/C<sub>2</sub>H<sub>4</sub> using ideal adsorbed solution theory (IAST) (Fig. S20–S22). At 298 K and 1 bar, the selectivities for the C<sub>2</sub>H<sub>2</sub>/C<sub>2</sub>H<sub>4</sub> (50/50, v/v) mixtures are 1.11 for **nia-d-TZB** and 1.45 for **nia-d-FTZB** (Fig. 3d). Under the same conditions, the selectivities for the C<sub>2</sub>H<sub>6</sub>/C<sub>2</sub>H<sub>4</sub> (50/50, 10/90, v/v) mixture are 1.58 for **nia-d-TZB** and 1.41 for **nia-d-FTZB** (Fig. 3d). These values are comparable to those of many benchmark ethane-selective



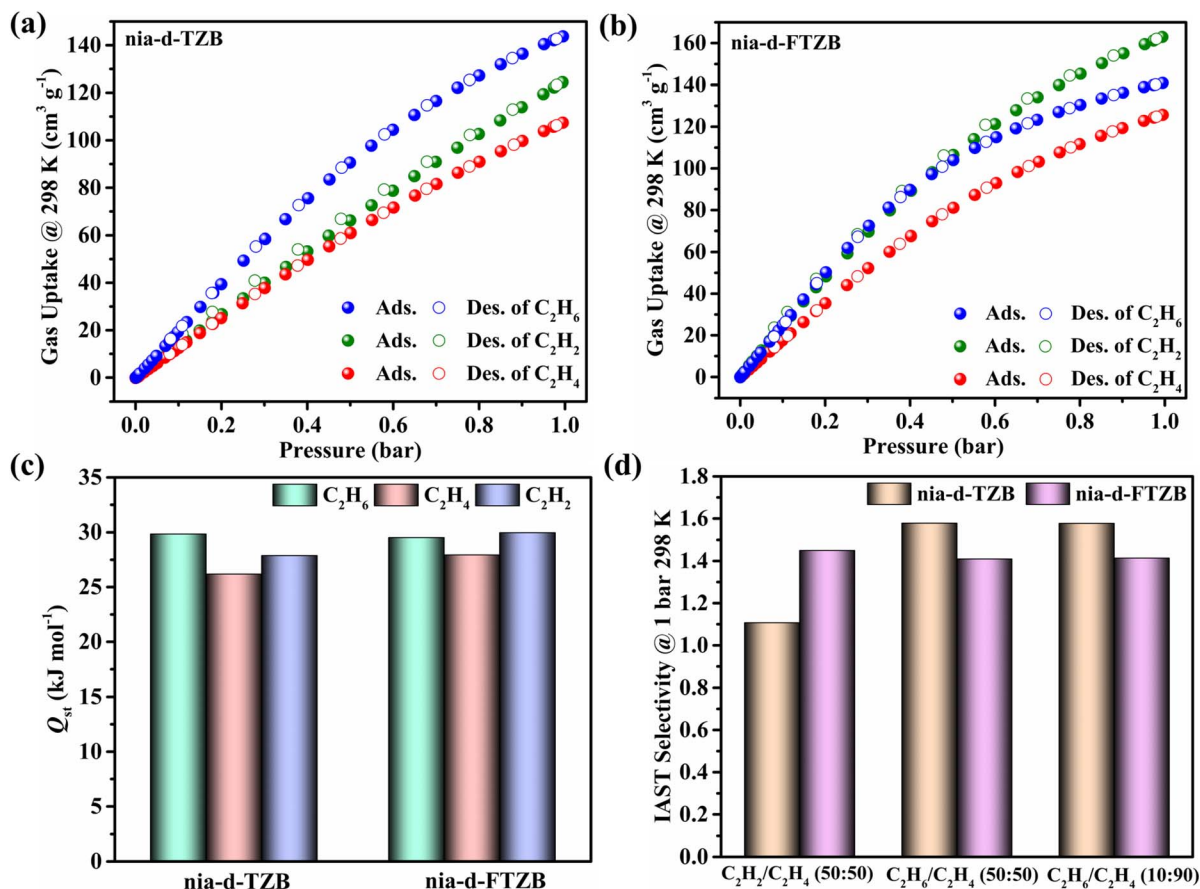


Fig. 3 (a) C<sub>2</sub>H<sub>2</sub>, C<sub>2</sub>H<sub>6</sub>, and C<sub>2</sub>H<sub>4</sub> sorption isotherms of nia-d-TZB at 298 K; (b) C<sub>2</sub> sorption isotherms of nia-d-FTZB at 298 K; (c)  $Q_{st}$  of C<sub>2</sub>H<sub>2</sub>, C<sub>2</sub>H<sub>6</sub> and C<sub>2</sub>H<sub>4</sub> for nia-d-TZB and nia-d-FTZB; (d) IAST selectivity of nia-d-TZB and nia-d-FTZB for C<sub>2</sub>H<sub>2</sub>/C<sub>2</sub>H<sub>4</sub> (50/50, v/v) and C<sub>2</sub>H<sub>6</sub>/C<sub>2</sub>H<sub>4</sub> (50/50, 10/90, v/v) at 298 K and 1 bar.

MOFs, such as Azole-Th-1 (1.46),<sup>57</sup> Zn-atz-oba (1.27),<sup>81</sup> JNU-2 (1.6),<sup>82</sup> and BF-108-Zn (1.37).<sup>83</sup> The results align with the observation that **nia-d-TZB** favors ethane removal from binary ethane/ethylene feeds, while **nia-d-FTZB** shows promise for simultaneous removal of acetylene and ethane from ternary C<sub>2</sub> mixtures, enabling one-step ethylene purification.

### Breakthrough experiment

To evaluate the practical separation performance, fixed-bed breakthrough experiments were performed with the samples activated at 120 °C. For **nia-d-TZB**, we first tested the binary C<sub>2</sub>H<sub>2</sub>/C<sub>2</sub>H<sub>4</sub> (50/50, v/v) and ternary C<sub>2</sub>H<sub>2</sub>/C<sub>2</sub>H<sub>6</sub>/C<sub>2</sub>H<sub>4</sub> (1/1/1, v/v/v) mixtures at 298 K and 1 bar with a total flow rate of 1.0 mL min<sup>-1</sup>. In two configurations, both C<sub>2</sub>H<sub>2</sub> and C<sub>2</sub>H<sub>4</sub> were observed at the outlet, indicating that no effective separation of the two components could be achieved under these conditions (Fig. 4a and S24). This result is consistent with the similar low-pressure isotherms for C<sub>2</sub>H<sub>2</sub> and C<sub>2</sub>H<sub>4</sub> and the modest difference in their adsorption affinities. In contrast, when the binary C<sub>2</sub>H<sub>6</sub>/C<sub>2</sub>H<sub>4</sub> mixtures (50/50, v/v) at the total flow-rates of 1.0 mL min<sup>-1</sup> were introduced into the fixed-bed, **nia-d-TZB** demonstrated a meaningful separation of C<sub>2</sub>H<sub>6</sub> from C<sub>2</sub>H<sub>4</sub> (Fig. 4b and S23). The breakthrough behaviour yielded a C<sub>2</sub>H<sub>6</sub>/

C<sub>2</sub>H<sub>4</sub> separation interval of about 6.4 min g<sup>-1</sup>. Notably, with a 10/90 (v/v) C<sub>2</sub>H<sub>6</sub>/C<sub>2</sub>H<sub>4</sub> feed and a flow rate of 1.0 mL min<sup>-1</sup>, C<sub>2</sub>H<sub>4</sub> began to emerge at the outlet around 78 min g<sup>-1</sup>, followed by a slower C<sub>2</sub>H<sub>6</sub> elution after ~19.1 min g<sup>-1</sup> (Fig. 4c and S23). The observed performance rivals several established ethane-selective materials reported in the literature, *e.g.*, JNU-2 (16 min g<sup>-1</sup>),<sup>82</sup> TKL-106 (15 min g<sup>-1</sup>),<sup>84</sup> UPC-612 (11.5 min g<sup>-1</sup>),<sup>85</sup> Zn-BPZ-TATB (14 min g<sup>-1</sup>),<sup>86</sup> NUM-9 (16 min g<sup>-1</sup>),<sup>87</sup> JNU-74 (22 min g<sup>-1</sup>),<sup>88</sup> and MOF-801 (20 min g<sup>-1</sup>).<sup>89</sup> The material demonstrated a C<sub>2</sub>H<sub>4</sub> production capacity of 17.19 L kg<sup>-1</sup>. These results demonstrate that **nia-d-TZB** can effectively separate C<sub>2</sub>H<sub>6</sub> from C<sub>2</sub>H<sub>4</sub> in binary feeds, enabling practical single-step ethylene purification from ethane-containing streams.

For **nia-d-FTZB**, breakthrough experiments were conducted similarly. In the binary C<sub>2</sub>H<sub>2</sub>/C<sub>2</sub>H<sub>4</sub> (50/50, v/v) test with a 1.0 mL min<sup>-1</sup> flow rate, C<sub>2</sub>H<sub>4</sub> eluted prior to C<sub>2</sub>H<sub>2</sub>, with C<sub>2</sub>H<sub>4</sub> breakthrough occurring at ~42 min g<sup>-1</sup> and C<sub>2</sub>H<sub>2</sub> subsequently reaching equilibrium after ~4.6 min g<sup>-1</sup> (Fig. 4d and S26). This demonstrates effective separation of acetylene from ethylene in this binary gas pair. We also tested the binary C<sub>2</sub>H<sub>6</sub>/C<sub>2</sub>H<sub>4</sub> (50/50, 10/90, v/v) feeds at 1.0 and 2.0 mL min<sup>-1</sup>. **nia-d-FTZB** showed a measurable separation performance for these two gases, with a separation interval of roughly 7.9 min g<sup>-1</sup> and 13.2 min g<sup>-1</sup>



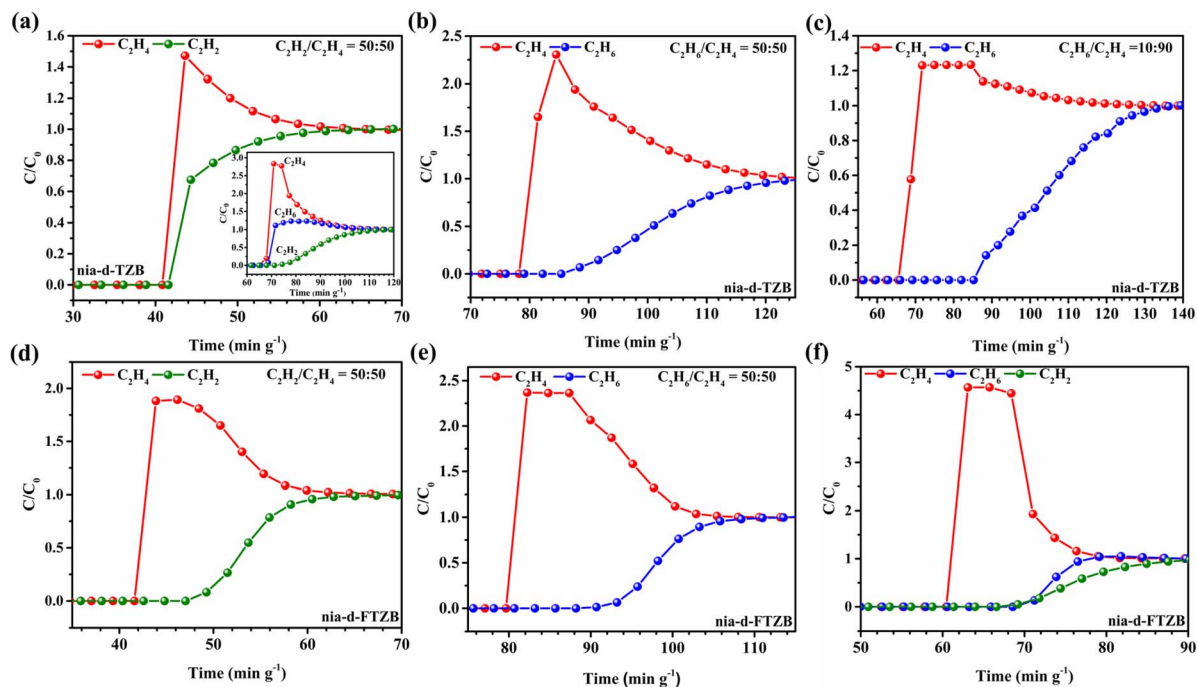


Fig. 4 Experimental breakthrough curves for **nia-d-TZB** at a total gas flow rate of  $1.0 \text{ mL min}^{-1}$  of (a)  $\text{C}_2\text{H}_2/\text{C}_2\text{H}_4$  (50/50, v/v) and  $\text{C}_2\text{H}_2/\text{C}_2\text{H}_4/\text{C}_2\text{H}_2$  (1/1/1, v/v/v), (b)  $\text{C}_2\text{H}_6/\text{C}_2\text{H}_4$  (50/50, v/v) and (c)  $\text{C}_2\text{H}_6/\text{C}_2\text{H}_4$  (10/90, v/v) at 298 K and 1 bar. Experimental breakthrough curves for **nia-d-FTZB** at a total gas flow rate of  $1.0 \text{ mL min}^{-1}$  of (d)  $\text{C}_2\text{H}_2/\text{C}_2\text{H}_4$  (50/50, v/v), (e)  $\text{C}_2\text{H}_6/\text{C}_2\text{H}_4$  (50/50, v/v) and (f)  $\text{C}_2\text{H}_6/\text{C}_2\text{H}_4/\text{C}_2\text{H}_2$  (1/1/1, v/v/v) at 298 K and 1 bar.

observed. With a 10/90 (v/v)  $\text{C}_2\text{H}_6/\text{C}_2\text{H}_4$  feed and a flow rate of  $1.0 \text{ mL min}^{-1}$ , the  $\text{C}_2\text{H}_4$  productivity reached  $11.88 \text{ L kg}^{-1}$ , confirming its ability to discriminate between  $\text{C}_2\text{H}_6$  and  $\text{C}_2\text{H}_4$  under practical flow conditions (Fig. 4e, S25 and S26).

To probe the full potential for ternary gas mixture separation, fixed-bed breakthrough experiments were performed with a  $\text{C}_2\text{H}_2/\text{C}_2\text{H}_6/\text{C}_2\text{H}_4$  (1/1/1, v/v/v) feed at 298 K and  $1.0 \text{ mL min}^{-1}$ . In this mixed-gas test,  $\text{C}_2\text{H}_4$  was detected at the outlet first (*i.e.*,  $61 \text{ min g}^{-1}$ ), followed by  $\text{C}_2\text{H}_6$  (after  $5.3 \text{ min g}^{-1}$ ), and finally  $\text{C}_2\text{H}_2$ , validating the potential for one-step ethylene purification in the presence of acetylene and ethane (Fig. 4f). The productivity of  $\text{C}_2\text{H}_4$  separation from the ternary mixture after the elution of  $\text{C}_2\text{H}_2$  and  $\text{C}_2\text{H}_6$  can be  $1.77 \text{ L kg}^{-1}$ .

The materials demonstrate outstanding regenerability, retaining high separation performance over multiple breakthrough cycles. Regeneration does not require heating. It only needs to be purged with  $10.0 \text{ mL min}^{-1}$  helium gas at 298 K for 30 minutes. Both **nia-d-TZB** and **nia-d-FTZB** exhibit exceptional cycling stability without noticeable degradation in adsorption capacity or selectivity across five times repeated runs (Fig. S26).

### GCMC simulation

To gain a deeper understanding of the selective adsorption and separation mechanism, modelling studies were conducted on **nia-d-TZB** and **nia-d-FTZB** using grand canonical Monte Carlo (GCMC) simulation. As illustrated in Fig. 5, the  $\text{C}_2$  gases are located at different positions within the framework of **nia-d-TZB**.  $\text{C}_2\text{H}_2$  and  $\text{C}_2\text{H}_4$  molecules exhibit similar adsorption positions and interaction features. Both gases are

predominantly distributed around the triangular windows, where  $\text{C}_2\text{H}_2$  molecules form  $\text{C-H}\cdots\text{N}$  interactions with nitrogen atoms in the tetrazole rings or TPT, with distances ranging from 3.33 to  $3.68 \text{ \AA}$ . Additionally, these molecules engage in  $\text{C-H}\cdots\pi$  interactions with pyridine rings on the TPT ligands, with an average distance of  $3.32 \text{ \AA}$  (Fig. 5a). Similarly,  $\text{C}_2\text{H}_4$  molecules occupy comparable binding sites, primarily interacting with tetrazole nitrogen atoms, benzene ring and TPT *via*  $\text{C-H}\cdots\pi$  and  $\text{C-H}\cdots\text{N}$  interactions, with distances ranging from  $3.43$  to  $3.50 \text{ \AA}$  and  $3.60$ – $3.98 \text{ \AA}$ , respectively (Fig. 5b). In contrast, the distribution of  $\text{C}_2\text{H}_6$  is distinct. These molecules are mainly localized at the metal cluster vertices, where they are surrounded by the framework, leading to stronger interactions. The primary binding sites for  $\text{C}_2\text{H}_6$  involve interactions with carboxylate oxygen atoms through  $\text{C-H}\cdots\text{O}$  hydrogen bonds (distances of  $3.01$ – $3.70 \text{ \AA}$ ) and with benzene rings *via*  $\text{C-H}\cdots\pi$  interactions (distances of  $3.21$ – $3.95 \text{ \AA}$ ) (Fig. 5c). The computational results indicate that **nia-d-TZB** exhibits stronger interactions with  $\text{C}_2\text{H}_6$  than with  $\text{C}_2\text{H}_4$  or  $\text{C}_2\text{H}_2$ , which aligns well with the experimental adsorption isotherms and the dynamic breakthrough results.

In contrast, all  $\text{C}_2$  molecules are located at the metal cluster vertices of **nia-d-FTZB**.  $\text{C}_2\text{H}_2$  and  $\text{C}_2\text{H}_6$  display similar adsorption behaviours and binding sites. Specifically,  $\text{C}_2\text{H}_2$  molecules form strong  $\text{C-H}\cdots\text{F}$  interactions with fluorine atoms on FTZB (distance:  $2.71 \text{ \AA}$ ),  $\text{C-H}\cdots\text{O}$  interactions with carboxylate oxygen (distance:  $3.88 \text{ \AA}$ ),  $\text{C-H}\cdots\text{N}$  interactions with tetrazole nitrogen atoms (distances:  $2.94$ – $3.85 \text{ \AA}$ ), and  $\text{C-H}\cdots\pi$  interactions with the tetrazole ring (distance:  $3.32 \text{ \AA}$ ) (Fig. 5d).  $\text{C}_2\text{H}_6$  molecules also form multiple hydrogen bonds with fluorine atoms and



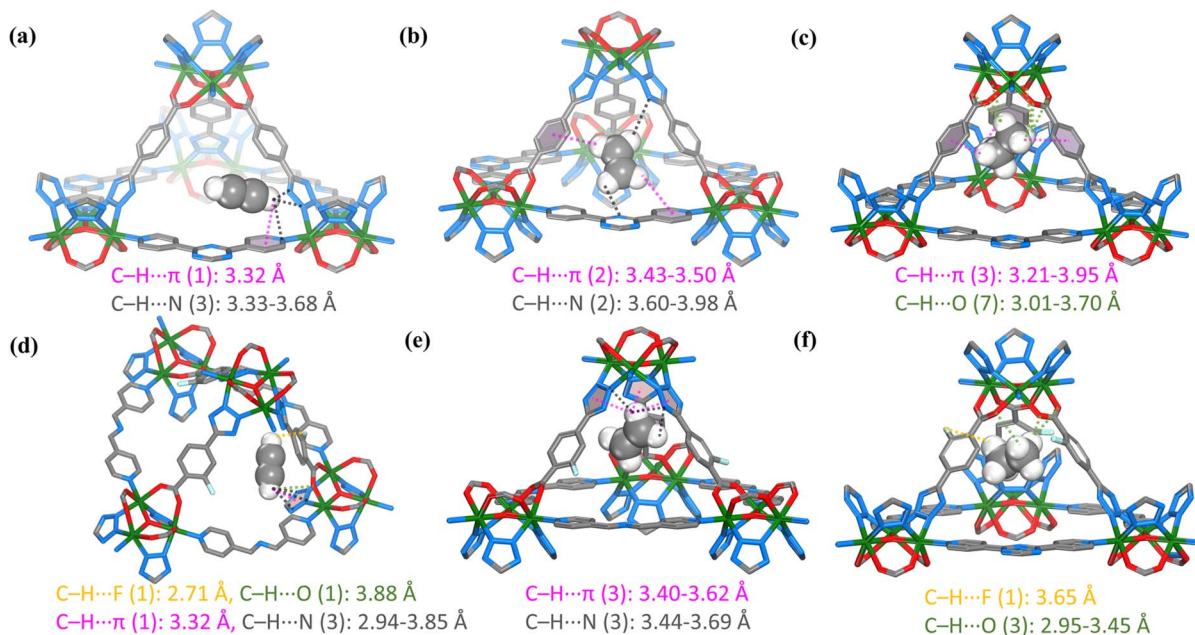


Fig. 5 The calculated preferential adsorption sites of **nia-d**-TZB for (a)  $C_2H_2$ , (b)  $C_2H_4$  and (c)  $C_2H_6$ . The calculated preferential adsorption sites of **nia-d**-FTZB for (d)  $C_2H_2$ , (e)  $C_2H_4$  and (f)  $C_2H_6$ . C: gray, Mn: green, O: red, N: sky blue, and F: light blue. The interactions are shown as dashed lines. For clarity, H atoms on frameworks are omitted.

carboxylate oxygen atoms, with interaction distances of  $C-H\cdots F$  at 3.65 Å and  $C-H\cdots O$  at 2.95–3.45 Å (Fig. 5f). The binding sites for  $C_2H_4$  differ significantly. These molecules primarily interact with the surrounding three tetrazole rings, forming relatively weak  $C-H\cdots\pi$  interactions with the tetrazole (distances: 3.40–3.62 Å) and multiple  $C-H\cdots N$  interactions with tetrazole nitrogen atoms (distances: 3.44–3.69 Å) (Fig. 5e). The calculated binding energies follow the order:  $C_2H_2$  (33.74 kJ mol<sup>-1</sup>) >  $C_2H_6$  (27.58 kJ mol<sup>-1</sup>) >  $C_2H_4$  (21.52 kJ mol<sup>-1</sup>). These results indicate that **nia-d**-FTZB exhibits strong and comparable adsorption capacities for  $C_2H_2$  and  $C_2H_6$ , with the strongest interaction observed for  $C_2H_2$  and the weakest for  $C_2H_4$ , consistent with the adsorption results.

Overall, computational findings confirm that both **nia-d**-TZB and **nia-d**-FTZB possess the capability for reverse separation of  $C_2H_6/C_2H_4$ . The introduction of fluorine atoms on the linear linkers modifies the chemical microenvironment as well as the interaction sites, subsequently strengthening the interactions between guest molecules and the framework. Therefore, **nia-d**-FTZB demonstrates the potential not only for the reverse separation of the binary  $C_2H_6/C_2H_4$  mixture, but also the one-step purification of  $C_2H_4$  from ternary  $C_2$  hydrocarbon mixtures.

## Conclusions

Leveraging reticular chemistry and a mixed-ligand strategy, two isorecticular, trinuclear-manganese-cluster-based, ternary MOFs, designated as **nia-d**-TZB and **nia-d**-FTZB, have been successfully synthesized. Both frameworks adopt the **nia-d** topology, a face-transitive net that endows the structures with a single window type. The strategic installation of fluorine atoms along the linear linker transforms TZB into FTZB, which

in turn elicits markedly divergent  $C_2$ -hydrocarbon sorption behaviours. In **nia-d**-TZB, acetylene and ethylene are taken up in comparable amounts, whereas ethane is adsorbed most strongly, enabling one-step ethylene purification from an ethane/ethylene binary mixture. In stark contrast, **nia-d**-FTZB exhibits the highest uptake for acetylene, followed by ethane, with ethylene being the least adsorbed. This hierarchy allows simultaneous removal of both acetylene and ethane from an acetylene/ethane/ethylene ternary stream, again delivering polymer-grade ethylene in a single step. Collectively, this work establishes a critical paradigm for the deliberate design of face-transitive MOFs that achieve advanced gas-separation performance, underscoring the potential of crystalline porous materials to contribute to energy savings and emission reductions.

## Author contributions

Wei-Hong Zhang: writing – original draft, supervision; Ya-Nan Ma: analysis of the single crystal structure; Guo-Tong Du: computational analysis; Ping Wang: performed a part of characterization of MOF materials; Dong-Xu Xue: writing – review & editing, supervision, data curation.

## Conflicts of interest

There are no conflicts to declare.

## Data availability

CCDC 2482490 and 2482491 contain the supplementary crystallographic data for this paper.<sup>90a,b</sup>



All experimental supporting data and procedures are available in the supplementary information (SI). Supplementary information is available. See DOI: <https://doi.org/10.1039/d5sc06836c>.

## Acknowledgements

We gratefully acknowledge the National Natural Science Foundation of China (No. 22471148 and 21871170), the National Key Research and Development Program of China (No. 2022YFA1205502), the Fundamental Research Funds for the Central Universities (No. GK202505027), and the Thousand Talents Program of Shaanxi Province and the Youth Innovation Team of Shaanxi Universities (2023).

## Notes and references

- 1 S. Chu, Y. Cui and N. Liu, *Nat. Mater.*, 2016, **16**, 16–22.
- 2 S. M. Sadrameli, *Fuel*, 2016, **173**, 285–297.
- 3 I. Amghizar, L. A. Vandewalle, K. M. Van Geem and G. B. Marin, *Engineering*, 2017, **3**, 171–178.
- 4 S. A. Chernyak, M. Corda, J. P. Dath, V. V. Ordonsky and A. Y. Khodakov, *Chem. Soc. Rev.*, 2022, **51**, 7994–8044.
- 5 D. S. Sholl and R. P. Lively, *Nature*, 2016, **532**, 435–437.
- 6 S. L. James, *Chem. Soc. Rev.*, 2003, **32**, 276–288.
- 7 J. R. Long and O. M. Yaghi, *Chem. Soc. Rev.*, 2009, **38**, 1213–1214.
- 8 B. Li, H. M. Wen, Y. Cui, W. Zhou, G. Qian and B. Chen, *Adv. Mater.*, 2016, **28**, 8819–8860.
- 9 H. C. Zhou and S. Kitagawa, *Chem. Soc. Rev.*, 2014, **43**, 5415–5418.
- 10 H. C. Zhou, J. R. Long and O. M. Yaghi, *Chem. Rev.*, 2012, **112**, 673–674.
- 11 Y. He, W. Zhou, T. Yildirim and B. Chen, *Energy Environ. Sci.*, 2013, **6**, 2735–2744.
- 12 K. G. Froudas, M. Vassaki, K. Papadopoulos, C. Tsangarakis, X. Chen, W. Shepard, D. Fairen-Jimenez, C. Tampaxis, G. Charalambopoulou, T. A. Steriotis and P. N. Trikalitis, *J. Am. Chem. Soc.*, 2024, **146**, 8961–8970.
- 13 L. Liang, C. Liu, F. Jiang, Q. Chen, L. Zhang, H. Xue, H. L. Jiang, J. Qian, D. Yuan and M. Hong, *Nat. Commun.*, 2017, **8**, 1233.
- 14 D. Sengupta, P. Melix, S. Bose, J. Duncan, X. Wang, M. R. Mian, K. O. Kirlikovali, F. Joodaki, T. Islamoglu, T. Yildirim, R. Q. Snurr and O. K. Farha, *J. Am. Chem. Soc.*, 2023, **145**, 20492–20502.
- 15 J. Zhou, Y. N. Ma, Y. F. Zhang, B. Zheng, K. Zheng, S. Liu, X. A. Guo, Y. B. Zhang and D. X. Xue, *J. Am. Chem. Soc.*, 2025, **147**, 21811–21817.
- 16 Y. Yabuuchi, H. Furukawa, K. M. Carsch, R. A. Klein, N. V. Tkachenko, A. J. Huang, Y. Cheng, K. M. Taddei, E. Novak, C. M. Brown, M. Head-Gordon and J. R. Long, *J. Am. Chem. Soc.*, 2024, **146**, 22759–22776.
- 17 R. C. Rohde, K. M. Carsch, M. N. Dods, H. Z. H. Jiang, A. R. McIsaac, R. A. Klein, H. Kwon, S. L. Karstens, Y. Wang, A. J. Huang, J. W. Taylor, Y. Yabuuchi, N. V. Tkachenko, K. R. Meihaus, H. Furukawa, D. R. Yahne, K. E. Engler, K. C. Bustillo, A. M. Minor, J. A. Reimer, M. Head-Gordon, C. M. Brown and J. R. Long, *Science*, 2024, **386**, 814–819.
- 18 S. Lu, Y.-J. Zhang, Y.-J. Cheng, Z.-H. Qin, G.-D. Wang, Y. Bai, Y. Lin, H. Wang, Y. Sui, L. Hou and Y.-Z. Li, *J. Mater. Chem. A*, 2025, **13**, 10581–10589.
- 19 Y. Ding, A. Dey, L. O. Alimi, P. M. Bhatt, J. Du, C. Maaliki, M. Eddaoudi, J. Jacquemin and N. M. Khashab, *Chem. Mater.*, 2021, **34**, 197–202.
- 20 M. Chang, F. Wang, Y. Wei, Q. Yang, J. X. Wang, D. Liu and J. F. Chen, *AIChE J.*, 2022, **68**, e17794.
- 21 K. B. Idrees, Z. Li, H. Xie, K. O. Kirlikovali, M. Kazem-Rostami, X. Wang, X. Wang, T. Y. Tai, T. Islamoglu, J. F. Stoddart, R. Q. Snurr and O. K. Farha, *J. Am. Chem. Soc.*, 2022, **144**, 12212–12218.
- 22 S. Capelo-Aviles, M. de Fez-Febre, S. R. G. Balestra, J. Cabezas-Gimenez, R. Tomazini de Oliveira, S. Gallo II, A. Vidal-Ferran, J. Gonzalez-Cobos, V. Lillo, O. Fabelo, E. C. Escudero-Adan, L. R. Falvello, J. B. Parra, P. Rumori, G. Turnes Palomino, C. Palomino Cabello, S. Giancola, S. Calero and J. R. Galan-Mascaros, *Nat. Commun.*, 2025, **16**, 3243–3258.
- 23 Y. Qi, C. Xue, Y. Zhang, Y. Huang, H. Huang, L. Gan and H. Yang, *ACS Mater. Lett.*, 2025, **7**, 1488–1495.
- 24 N. Sun, X. Zhou, J. Liu, H. Yu, X. Si, F. Ding and Y. Sun, *J. Mater. Chem. A*, 2025, **13**, 9665–9672.
- 25 D.-H. Nam, O. Shekhah, A. Ozden, C. McCallum, F. Li, X. Wang, Y. Lum, T. Lee, J. Li, J. Wicks, A. Johnston, D. Sinton, M. Eddaoudi and E. H. Sargent, *Adv. Mater.*, 2022, **34**, 2207088.
- 26 Y. L. Li, N. Li, Z. B. Mei, J. R. Li, S. J. Yao, F. Yu, S. L. Li, J. M. Lin, J. Liu and Y. Q. Lan, *Chem. Sci.*, 2025, **16**, 11939–11948.
- 27 Y. Liang, H. Zhou, Y. Zhao, X. Liang, Z. Chen, M. Ji and M. Wang, *Chem. Sci.*, 2025, **16**, 15223–15230.
- 28 A. Pal, S. Suresh, A. Khan, L. H. Kuo, L. T. Chi, A. Ganguly, C. Y. Kao, M. K. Sharma, T. S. A. Wang, D. Y. Kang and Z. H. Lin, *Sci. Adv.*, 2025, **11**, eads4711.
- 29 Y.-Y. Tang, X. Luo, R.-Q. Xia, J. Luo, S.-K. Peng, Z.-N. Liu, Q. Gao, M. Xie, R.-J. Wei, G.-H. Ning and D. Li, *Angew. Chem., Int. Ed.*, 2024, **63**, e202408186.
- 30 K. Gupta and A. K. Patra, *ACS Sens.*, 2020, **5**, 1268–1272.
- 31 J. Wang, Y. Cheng, J. Zhou and W. Tang, *J. Mater. Chem. C*, 2021, **9**, 12086–12093.
- 32 S. Ghosh, R. Lipin, A. Ngoipala, N. Ruser, D. M. Venturi, A. Rana, M. Vandichel and S. Biswas, *Inorg. Chem.*, 2023, **62**, 14632–14646.
- 33 J. Y. M. Chan, E. O. Shehayeb, D. L. Pennington, C. H. Hendon and K. A. Mirica, *J. Am. Chem. Soc.*, 2025, **147**, 29003–29012.
- 34 Y. Shen, A. Tissot and C. Serre, *Chem. Sci.*, 2022, **13**, 13978–14007.
- 35 Z. Han, K. Y. Wang, R. R. Liang, Y. Guo, Y. Yang, M. Wang, Y. Mao, J. Huo, W. Shi and H. C. Zhou, *J. Am. Chem. Soc.*, 2025, **147**, 3866–3873.
- 36 M. Ran, Y. Liu, L. Feng, J. Ning, J. Li and X. Dou, *ACS Appl. Nano Mater.*, 2025, **8**, 8231–8240.



- 37 P. Horcajada, T. Chalati, C. Serre, B. Gillet, C. Sebrie, T. Baati, J. F. Eubank, D. Heurtaux, P. Clayette, C. Kreuz, J. S. Chang, Y. K. Hwang, V. Marsaud, P. N. Bories, L. Cynober, S. Gil, G. Ferey, P. Couvreur and R. Gref, *Nat. Mater.*, 2010, **9**, 172–178.
- 38 X.-X. Zeng, J.-S. Lu, D.-W. Ma, Y.-T. Huang, L. Chen, G. Wang, Q. Chen and N. Lin, *Rare Met.*, 2024, **43**, 4867–4883.
- 39 J. R. Li, R. J. Kuppler and H. C. Zhou, *Chem. Soc. Rev.*, 2009, **38**, 1477–1504.
- 40 Z. Bao, G. Chang, H. Xing, R. Krishna, Q. Ren and B. Chen, *Energy Environ. Sci.*, 2016, **9**, 3612–3641.
- 41 H. Li, K. Wang, Y. Sun, C. T. Lollar, J. Li and H.-C. Zhou, *Mater. Today*, 2018, **21**, 108–121.
- 42 R.-B. Lin, S. Xiang, W. Zhou and B. Chen, *Chem*, 2020, **6**, 337–363.
- 43 L. Yang, S. Qian, X. Wang, X. Cui, B. Chen and H. Xing, *Chem. Soc. Rev.*, 2020, **49**, 5359–5406.
- 44 L. Yang, P. Zhang, J. Cui, X. Cui and H. Xing, *Angew. Chem., Int. Ed.*, 2024, **63**, e202414503.
- 45 C. Gücüyener, J. van den Bergh, J. Gascon and F. Kapteijn, *J. Am. Chem. Soc.*, 2010, **132**, 17704–17706.
- 46 P. Q. Liao, W. X. Zhang, J. P. Zhang and X. M. Chen, *Nat. Commun.*, 2015, **6**, 8697.
- 47 H. G. Hao, Y. F. Zhao, D. M. Chen, J. M. Yu, K. Tan, S. Ma, Y. Chabal, Z. M. Zhang, J. M. Dou, Z. H. Xiao, G. Day, H. C. Zhou and T. B. Lu, *Angew. Chem., Int. Ed.*, 2018, **57**, 16067–16071.
- 48 Y. Chen, Z. Qiao, H. Wu, D. Lv, R. Shi, Q. Xia, J. Zhou and Z. Li, *Chem. Eng. Sci.*, 2018, **175**, 110–117.
- 49 Y. Han, L. Meng, Y. Liu, H. Li, Z. Ji, Y. Zhou, M. Wu and Z. Han, *Sep. Purif. Technol.*, 2023, **315**, 123642.
- 50 L. Li, R. B. Lin, R. Krishna, H. Li, S. Xiang, H. Wu, J. Li, W. Zhou and B. Chen, *Science*, 2018, **362**, 443–446.
- 51 M. Li, L. Yin, S. Li, J. Miao, Z. Wang and H. Wang, *Inorg. Chem.*, 2025, **64**, 12440–12445.
- 52 S. M. Wang, M. Shivanna, S. T. Zheng, T. Pham, K. A. Forrest, Q. Y. Yang, Q. Guan, B. Space, S. Kitagawa and M. J. Zaworotko, *J. Am. Chem. Soc.*, 2024, **146**, 4153–4161.
- 53 Y. Wang, F. Zhang, Y. Yang, X. Wang, L. Li, J. Li and J. Yang, *J. Colloid Interface Sci.*, 2025, **687**, 439–448.
- 54 F. Xie, J. Liu, W. Graham, S. Ullah, E. M. Cedeño Morales, K. Tan, T. Thonhauser, H. Wang and J. Li, *Chem. Eng. J.*, 2023, **473**, 145096.
- 55 Y. Ye, Y. Xie, Y. Shi, L. Gong, J. Phipps, A. M. Al-Enizi, A. Nafady, B. Chen and S. Ma, *Angew. Chem., Int. Ed.*, 2023, **62**, e202302564.
- 56 L. P. Zhang, G. W. Guan, Y. T. Li, H. R. Liu, S. T. Zheng, Y. Jiang, R. Bai and Q. Y. Yang, *Small*, 2024, **20**, e2402382.
- 57 Z. Xu, X. Xiong, J. Xiong, R. Krishna, L. Li, Y. Fan, F. Luo and B. Chen, *Nat. Commun.*, 2020, **11**, 3163.
- 58 B. Zhu, J. W. Cao, S. Mukherjee, T. Pham, T. Zhang, T. Wang, X. Jiang, K. A. Forrest, M. J. Zaworotko and K. J. Chen, *J. Am. Chem. Soc.*, 2021, **143**, 1485–1492.
- 59 G. D. Wang, Y. Z. Li, W. J. Shi, L. Hou, Y. Y. Wang and Z. Zhu, *Angew. Chem., Int. Ed.*, 2022, **61**, e202205427.
- 60 J. Liu, H. Wang and J. Li, *Chem. Sci.*, 2023, **14**, 5912–5917.
- 61 Z. Ji, Q. Li, Y. Zhou, R. Krishna, M. Hong and M. Wu, *Angew. Chem., Int. Ed.*, 2024, **63**, e202411175.
- 62 X. Jiang, Y. Wang, H. Wang, L. Cheng, J. W. Cao, J. B. Wang, R. Yang, D. H. Zhang, R. Y. Zhang, X. B. Yang, S. H. Wang, Q. Y. Zhang and K. J. Chen, *Nat. Commun.*, 2025, **16**, 694–704.
- 63 Q. Ding, Z. Zhang, Y. Liu, K. Chai, R. Krishna and S. Zhang, *Angew. Chem., Int. Ed.*, 2022, **61**, e202208134.
- 64 Y. N. Ma, T. L. Liu, W. H. Zhang, C. H. He and D. X. Xue, *Angew. Chem., Int. Ed.*, 2025, **64**, e202513208.
- 65 O. Delgado Friedrichs, M. O’Keeffe and O. M. Yaghi, *Acta Crystallogr., Sect. A: Found. Adv.*, 2003, **59**, 515–525.
- 66 N. W. Ockwig, O. Delgado-Friedrichs, M. O’Keeffe and O. M. Yaghi, *Acc. Chem. Res.*, 2005, **38**, 176–182.
- 67 O. Delgado-Friedrichs, M. O’Keeffe and O. M. Yaghi, *Acta Crystallogr., Sect. A: Found. Adv.*, 2006, **62**, 350–355.
- 68 J. Kim and W. Choe, *Chem*, 2022, **8**, 617–631.
- 69 P. M. Bhatt, V. Guillermin, S. J. Datta, A. Shkurenko and M. Eddaoudi, *Chem*, 2020, **6**, 1613–1633.
- 70 M. O’Keeffe, M. A. Peskov, S. J. Ramsden and O. M. Yaghi, *Acc. Chem. Res.*, 2008, **41**, 1782–1789.
- 71 Y. Ye, Z. Ma, R. B. Lin, R. Krishna, W. Zhou, Q. Lin, Z. Zhang, S. Xiang and B. Chen, *J. Am. Chem. Soc.*, 2019, **141**, 4130–4136.
- 72 L. Liu, Z. Yao, Y. Ye, Y. Yang, Q. Lin, Z. Zhang, M. O’Keeffe and S. Xiang, *J. Am. Chem. Soc.*, 2020, **142**, 9258–9266.
- 73 A. N. Hong, H. Yang, X. Bu and P. Feng, *EnergyChem*, 2022, **4**, 100080.
- 74 X. Mu, Y. Xue, M. Hu, P. Zhang, Y. Wang, H. Li, S. Li and Q. Zhai, *Chin. Chem. Lett.*, 2023, **34**, 107296.
- 75 Y. Zhang, Y. Han, B. Luan, L. Wang, W. Yang, Y. Jiang, T. Ben, Y. He and B. Chen, *J. Am. Chem. Soc.*, 2024, **146**, 17220–17229.
- 76 Y. Z. Hao, K. Shao, X. Zhang, Y. H. Yu, D. Liu, H. M. Wen, Y. Cui, B. Li, B. Chen and G. Qian, *J. Am. Chem. Soc.*, 2025, **147**, 11257–11266.
- 77 W. Wang, Y. Chen, K. X. Phan, Z. Jia, Y. Xiao, X. Bu and P. Feng, *J. Am. Chem. Soc.*, 2025, **147**, 31239–31248.
- 78 Y. W. Chen, Z. W. Qiao, H. X. Wu, D. F. Lv, R. F. Shi, Q. B. Xia, J. Zhou and Z. Li, *Chem. Eng. Sci.*, 2018, **175**, 110–117.
- 79 H. M. Wen, C. Yu, M. Liu, C. Lin, B. Zhao, H. Wu, W. Zhou, B. Chen and J. Hu, *Angew. Chem., Int. Ed.*, 2023, **62**, e202309108.
- 80 X. W. Gu, J. X. Wang, E. Wu, H. Wu, W. Zhou, G. Qian, B. Chen and B. Li, *J. Am. Chem. Soc.*, 2022, **144**, 2614–2623.
- 81 J. W. Cao, S. Mukherjee, T. Pham, Y. Wang, T. Wang, T. Zhang, X. Jiang, H. J. Tang, K. A. Forrest, B. Space, M. J. Zaworotko and K. J. Chen, *Nat. Commun.*, 2021, **12**, 6507–6515.
- 82 H. Zeng, X. J. Xie, M. Xie, Y. L. Huang, D. Luo, T. Wang, Y. Zhao, W. Lu and D. Li, *J. Am. Chem. Soc.*, 2019, **141**, 20390–20396.
- 83 Q. L. Hong, W. J. Wang, S. M. Chen, K. Chen, M. Liu, H. X. Zhang and J. Zhang, *Chem. Mater.*, 2022, **34**, 307–313.
- 84 M. H. Yu, H. Fang, H. L. Huang, M. Zhao, Z. Y. Su, H. X. Nie, Z. Chang and T. L. Hu, *Small*, 2023, **19**, 2300821.



- 85 Y. Wang, C. Hao, W. Fan, M. Fu, X. Wang, Z. Wang, L. Zhu, Y. Li, X. Lu, F. Dai, Z. Kang, R. Wang, W. Guo, S. Hu and D. Sun, *Angew. Chem., Int. Ed.*, 2021, **60**, 11350–11358.
- 86 G. D. Wang, Y. Z. Li, W. J. Shi, L. Hou, Y. Y. Wang and Z. Zhu, *Angew. Chem., Int. Ed.*, 2023, **62**, e202311654.
- 87 S. Q. Yang, F. Z. Sun, P. Liu, L. Li, R. Krishna, Y. H. Zhang, Q. Li, L. Zhou and T. L. Hu, *ACS Appl. Mater. Interfaces*, 2021, **13**, 962–969.
- 88 G. D. Wang, Y. Z. Li, H. Zeng, L. Hou, W. G. Lu and D. Li, *Adv. Funct. Mater.*, 2025, **35**, 2504916.
- 89 F. Xie, J. Q. Liu, W. Graham, S. Ullah, E. M. C. Morale, K. Tan, T. Thonhauser, H. Wang and J. Li, *Chem. Eng. J.*, 2023, **473**, 145096.
- 90 (a) CCDC 2482490: Experimental Crystal Structure Determination, 2025, DOI: [10.5517/ccdc.csd.cc2pb7bm](https://doi.org/10.5517/ccdc.csd.cc2pb7bm); (b) CCDC 2482491: Experimental Crystal Structure Determination, 2025, DOI: [10.5517/ccdc.csd.cc2pb7cn](https://doi.org/10.5517/ccdc.csd.cc2pb7cn).

